ACS APPLIED MATERIALS & INTERFACES

Research Article

www.acsami.org

Carbon Nanotube Balls and Their Application in Supercapacitors

Da-Young Kang and Jun Hyuk Moon*

Department of Chemical and Biomolecular Engineering, Sogang University, Seoul, 121-742, Republic of Korea

Supporting Information

ABSTRACT: We have provided a design of the macroscopic morphology of carbon nanotubes (CNTs) using emulsion droplet confinement. The evaporation of CNT-dispersed aqueous emulsion droplets in oil produces spherical CNT assemblies, i.e., CNT balls. In this emulsion-assisted method, compact packing of CNT was obtained by the presence of capillary pressure during droplet evaporation. The size of the CNT balls could be controlled by changing the concentration of the CNT dispersion solution; typically, CNT balls with an average size in the range of 8−12 μm were obtained with a Brunauer−Emmett−Teller (BET) specific area of 200 m^2/g. Heat treatment of the CNT balls, which was required to remove residual solvent, and cement CNTs was followed, and their effect has been characterized; the heat treatment at high temperature desorbed surface oxygenated groups of CNTs and created defective carbon structures, but did not change pore structure. The dispersion of CNT balls was applied to form CNT ball-assembled film for a supercapacitor electrode. The specific capacitance of 80 F/g was obtained at 500 °C heat treatment, but the CNT balls prepared at a higher temperature actually decreased the capacitance, because of the removal of surface oxygenated groups, thereby decreasing the pseudo-capacitance. The capacitive properties of CNT ball-assembled electrodes were compared to CNT films; the CNT ball electrodes showed 40% higher specific electrochemical capacitance and higher rate performance, which is attributed to the compact packing of CNTs in the CNT ball and the hierarchical porous structures in the ball assemblies.

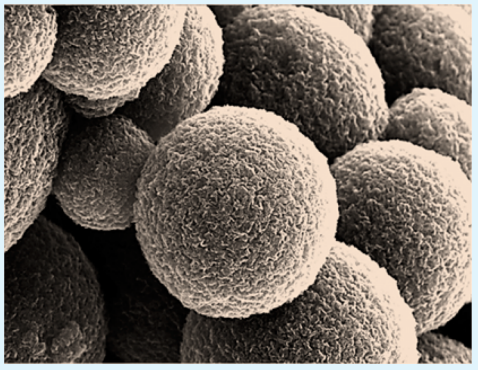

KEYWORDS: *carbon nanotubes, carbon nanotube assemblies, confinement geometry, emulsion, supercapacitor*

INTRODUCTION

Carbon nanotubes (CNTs) are attractive materials for use as the electrodes in electrochemical energy storage devices, such as supercapacitors,[1−4] lithium-ion batteries,[5−7] and fuel cells,[8,9] because of their high chemical stability, electrical conductivity, accessible surface area, and facile functionalization.[10−12] CNTs have unique morphological characteristics: they possess a central canal pore, and percolating CNT networks can create an interconnected pore network. Thus, the pore structures of CNTs increase the contact area with an electrolyte solution which facilitates ion transport, thereby improving the performance of those electrochemical devices that make use of them, as opposed to those using other carbon materials, such as activated carbons.[13,14] For example, activated carbon, which has often been used as a conventional electrode, was reported to have a specific area of up to 2000 m^2/g and yield a specific capacitance of up to 100 F/g in an aqueous electrolyte solution.[15,16] On the other hand, CNTs possess a relatively small specific area, in the range of 200−400 m^2/g, but show a specific capacitance comparable to that of activated carbons. The maximum specific capacitance of a multiwalled carbon nanotube (MWCNT) film reported to date is ∼100 F/g, and capacitance values have varied widely, depending on the type of nanotube, the electrolyte solution, the use of an activation process or not, and the presence or absence of binders.[14,17,18] Moreover, the facile composites that comprise CNTs and oxides (e.g., RuO_2, MnO_2, NiO) or conducting polymers (e.g., polypyrrole, polyaniline) may display improved capacitance values, because of a pseudo-faradaic reaction.[3,5,19−22]

Control over the macroscopic shapes of CNT assemblies plays a crucial role in their practical application. CNTs have been prepared in the form of a fiber or yarn for mechanical applications or as woven textiles for the preparation of electrodes.[23,24] CNT mats or sheets have been prepared for electrochemical applications.[25] The liquid-induced collapse of vertically aligned CNT arrays grown directly on the substrate has provided a facile method for designing CNT assemblies.[26,27] Using this approach, highly dense CNTs have been obtained and have proven advantageous for use in supercapacitor applications.[26] Consistent with these approaches toward the design of macroscopic morphologies, we have demonstrated the fabrication of spherical CNT assemblies. CNT-dispersed emulsion droplets were used to confine the geometry of the CNT suspension, yielding spherical CNTs (CNT balls). The emulsion-assisted method yielded compact packing of the dispersant; that is, CNT assemblies were obtained under the inward capillary pressure exerted by the shrinkage of a droplet during evaporation.[28] Moreover, the CNT balls could be re-suspended to form a dispersion that facilitated the application of the CNT balls in the substrate

Received: November 5, 2013
Accepted: December 12, 2013
Published: December 23, 2013

 © 2013 American Chemical Society

coating. The CNT ball assemblies were then tested for their utility as an electrode material in a supercapacitor. The electrochemical capacitance of the CNT ball-assembled electrodes was compared to the performances of the CNT films. The CNT ball electrodes displayed a 40% higher specific capacitance and a slightly higher rate performance, possibly attributed to the compact packing of CNTs and the formation of hierarchical porous structures.

METHODS

Preparation of the Carbon Nanotube Balls. Water-dispersed MWCNTs (Hanhwa Nanotech) were added to hexadecane (Aldrich) containing 1 wt % surfactant (Hypermer 2296, Croda), and the mixture was vigorously vortexed for 10 min to obtain the water-in-oil emulsion. The water inside the droplet was efficiently dried by pouring the emulsion into a Teflon dish and drying in a convection oven at 60 °C for 24 h. The dried CNT assemblies were rinsed with propylene glycol methyl ether acetate (PGMEA, Aldrich) several times and dried in a vacuum oven for a day. The CNT balls were heat-treated in a furnace under inert conditions at three different temperatures: 500, 700, and 900 °C for 2 h. The heating rates were 3 °C/min.

Characterization. Optical microscopy images were obtained using an optical microscope (Nikon LV100) equipped with a digital camera. SEM images were obtained using a Hitachi Model S-4300 scanning electron microscope at 4.8 kV. Transmission electron microscopy images were obtained using a Carl Zeiss Model LIBRA 120 instrument operated at 120 kV. The measurements were obtained by heating the sample up to 900 °C in a nitrogen atmosphere, with a heating rate of 3 °C/min. The Raman spectra were collected using a Horiba Jobin Yvon LabRAM HR equipped with an air-cooled Ar-ion laser operated at 541 nm. X-ray photoelectron spectroscopy (XPS) was performed using a Leybold spectrometer with an Al Kα monochromatic beam (1486.6 eV) having an input power of 150 W (ESCALAB250 XPS system, Theta Probe XPS system). Nitrogen adsorption isotherms were recorded using a Micromeritics Model ASAP 2405N. Specific surface areas were calculated by the Brunauer–Emmett–Teller (BET) method, and pore volumes were estimated from pore size distribution curves obtained from the desorption branches of the isotherms using the Barrett–Joyner–Halenda (BJH) method.

Electrochemical Measurements. A beaker-type three-electrode system was used to measure the electrochemical properties of the sample. The three-electrode cell was assembled with CNT ball-assembled films on a glassy electrode as the working electrode, a saturated Ag/AgCl electrode (3 M NaCl) as the reference, and a Pt rod as the counter electrode. Specifically, the working electrode was prepared by casting a Nafion-impregnated sample onto a glassy carbon electrode. Four milliliters (4 mL) of an aqueous ethanol solution in which 10 mg of the sample was dispersed was dropped onto the glassy carbon electrode and placed in a convection oven until the sample was dried. The working electrode was then immersed in a 1.0 M H_2SO_4 (Aldrich) solution. Cyclic voltammetry (CV) and galvanostatic charge–discharge cycles were measured by VersaSTAT 3 (AMETEK). CV was performed over the voltage range of 0 to 1 V with a range of scan rates (from 0.01 V/s to 1 V/s). The charge-discharge measurement was performed over the voltage between 0 and 1 V with applying a constant current of 1 A/g.

RESULTS AND DISCUSSION

The fabrication of CNT balls using emulsion-directed assembly is described in Scheme 1. First, an aqueous emulsion droplet of a CNT dispersion (MWCNTs with an average diameter of 12 nm) was prepared in hexadecane in the presence of 1 wt % non-ionic surfactant. Upon heating the emulsion, the water slowly evaporated from the hexadecane while the CNTs assembled within the spherically confined volume, yielded CNT balls in the hexadecane. The CNT balls were washed with PGMEA to remove solvent and surfactant residue. A CNT ball powder was subsequently obtained by heat treatment under inert conditions. The CNT balls were dispersed in a water–ethanol mixture to prepare an electrode film for supercapacitor electrodes.

Scheme 1. Emulsion-Directed Assembly of CNT Balls and Their Dispersion in Solution

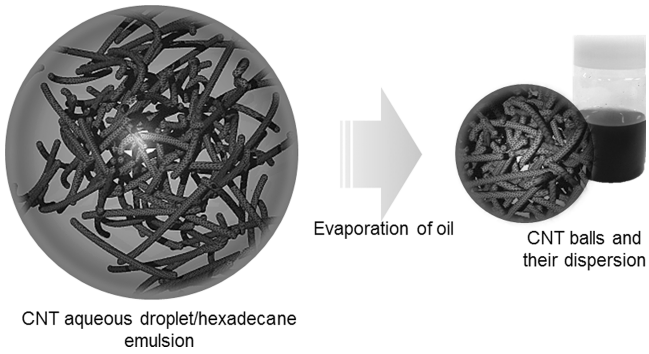

Figure 1a shows scanning electrode microscopy (SEM) images of the CNT balls. The diameters of the emulsion droplets (the inset image) and CNT balls after the drying out of these droplets were 20 ± 5 μm and 10 ± 3 μm, respectively. The concentration (C) and density (ρ_0) of the CNT dispersion was 2 wt % and ~0.02 g/cm^3. Assuming that the density (ρ) of MWCNT was 0.1–0.3 g/cm^3 and the porosity (φ) of the MWCNT film was 50%–60%, the volume of CNT balls (V_{ball})

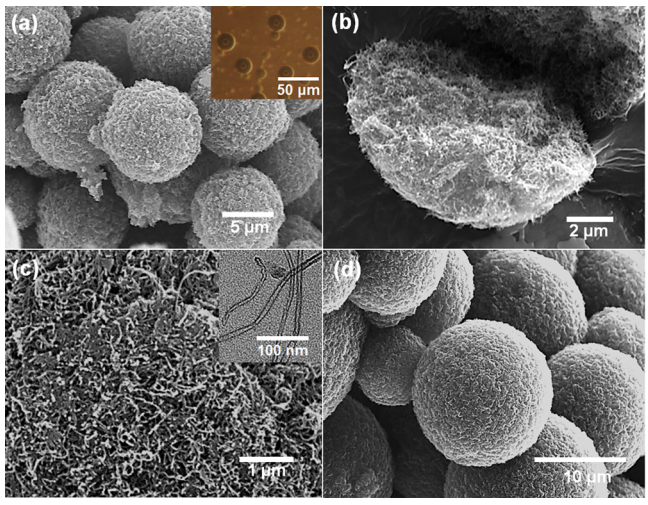

Figure 1. SEM images of the (a) CNT balls and (b) the inside of a broken CNT ball. (c) A magnified SEM image of the CNT ball surface (inset image shows a TEM image of the MWCNTs). (d) SEM image of the CNT balls fabricated using a high concentration of CNT dispersion.

dx.doi.org/10.1021/am404960r | ACS Appl. Mater. Interfaces 2014, 6, 706–711

was expected to be $C\rho_0 V_{drop}/\rho\varphi$. The estimated diameter of the CNT balls was 10 ± 3 μm, similar to the diameter of the fabricated structures. These results indicate that the CNT balls may have been condensed without forming a large internal cavity, and compact packing inside the balls was confirmed, as shown in the inset image of Figure 1b. Magnified SEM images of the CNT balls in Figure 1c reveal a compact percolating network of CNTs. The size of the CNT balls could be controlled according to the initial size of the emulsion droplet and the concentration of the CNT dispersion. The concentration of the CNT dispersion was 6 wt %, which yielded CNT balls with larger diameters of 15 ± 3 μm (Figure 1d). The capillary pressure exerted by the evaporation of a water droplet may enhance the packing of CNTs. We compared the morphology of a CNT film after the evaporation of a CNT dispersion in water or in ethanol, as shown in Figure S1 in the Supporting Information. The CNTs obtained from the ethanol dispersion had relatively larger pores around the CNTs. This structural feature was attributed to the lower surface tension of ethanol compared to water, which meant that the ethanol droplet exerted a lower capillary pressure. The high density of the CNT percolating network is attractive for electrochemical applications because higher densities can enhance the energy density and a high connectivity among CNTs can increase the conductivity of the CNT assemblies.[26]

Heat treatment of the CNT balls was required to remove the surfactants and hexadecane from the CNT balls. Heat treatment may also change the functional groups on the CNT surfaces, the pores and specific areas of the CNT films, and induce further graphitization of the CNTs, which are critical properties for supercapacitor applications of CNT balls.[14] Results from the thermogravimetric analysis (TGA) of the CNT balls are shown in Figure S2 in the Supporting Information. Most of the organic residue and/or solvent captured inside the CNT balls were removed at temperatures beyond 400 °C in a nitrogen atmosphere, and only a 5% mass loss was observed upon heating to 900 °C. The specific area and pore volume of the CNT balls were characterized by the BET method. Nitrogen isotherms for the CNT balls at various temperatures are presented in Figure 2. The BET surface area, pore area, and pore volume were estimated from the pore size distribution curves from the desorption branches of the isotherms using the BJH method, as summarized in Table 1. The isotherms were Type IV with a Type H4 hysteresis, which suggests the presence of mesopores in the CNT balls.[29] Table 1 shows that the CNT balls prepared at various temperatures exhibited similar specific areas and pore volumes: specific area of 200–220 m^2/g and a pore volume of 0.5–0.6 m^3/g. The heat treatment did not appear to influence the percolated morphologies of the CNT structures.

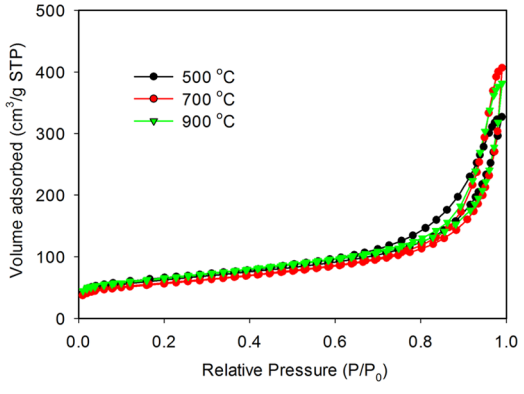

Figure 2. BET isotherms of the CNT balls prepared at various temperatures.

Table 1. Pore Characteristics of the CNT Balls Prepared at Various Temperatures: Brunauer–Emmett–Teller (BET) Surface Area, Micropore Area Estimated by the BET Method, Mesopore Area Estimated by the Barrett–Joyner–Halenda (BJH) Method, and Total Pore Volume

temperature [°C]	BET surface area [m^2/g]	micropore area [m^2/g]	mesopore area [m^2/g]	total pore volume [cm^3/g]
500	222.52	61.72	192.16	0.51
700	200.32	55.51	170.18	0.61
900	228.60	66.32	186.94	0.59

Figure 3 shows the Raman spectra at various temperatures, which were collected to characterize the effects of heat treatment on the carbon nanostructures. The spectra exhibited two peaks, at 1350 and 1580 cm^{-1}, which were designated as the D-band and G-band, respectively. The G-band is associated with the vibrational modes of the sp^2-bonded carbon atoms in a graphitic layer, whereas the D-band indicates the presence of defects in the graphene lattice.[30,31] A comparison of the intensity ratio of the D- and G-bands (I_D/I_G) showed that the value of I_D/I_G increased as the heat-treatment temperature increased, indicating a decrease in the average size of the sp^2 domains. Figure 4a shows representative X-ray photoelectron spectroscopy (XPS) results obtained from CNT balls treated at 500 °C. The C 1s band was deconvoluted into the following bands: carbon in aromatic rings (i.e., C–C) at 284.5 eV, carbon singly bound to oxygen epoxy or alkoxy groups (i.e., C–O) at 285.5 eV, carbon doubly bound to oxygen in carbonyl or carboxylic groups (i.e., C═O) at 287.0 eV, carbon bound to two oxygen atoms in carboxyl, carboxylic anhydrides, or ester groups (i.e., –COO) at 288.6 eV, and the characteristic aromatic $\pi-\pi^*$ transition at 289.9 eV.[32,33] Figure 4b shows the changes in the quantity of each functional group present upon heating at various temperatures, as estimated by the area ratios of each oxygenated functional peak to the area of the C–C peak. Overall, a large decrease in the oxygen content was observed during heat treatment in an inert environment. Specifically, the functional groups having C–O bonds were

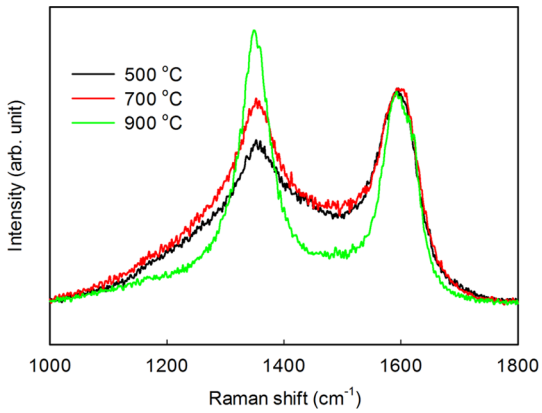

Figure 3. Raman spectra of the CNT balls prepared at various temperatures.

dx.doi.org/10.1021/am404960r | ACS Appl. Mater. Interfaces 2014, 6, 706–711

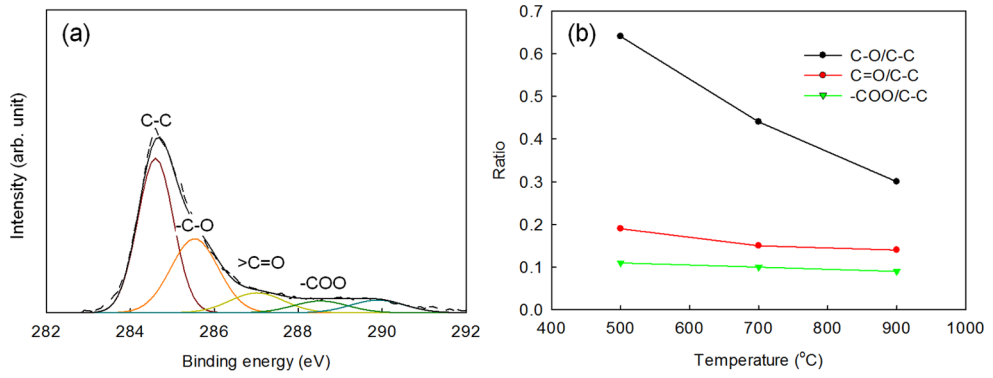

Figure 4. (a) XPS C 1s deconvoluted spectra of CNT balls treated at 500 °C. (b) Atomic ratios of the different functional groups, relative to graphitic carbon, varied depending on the heat-treatment temperature.

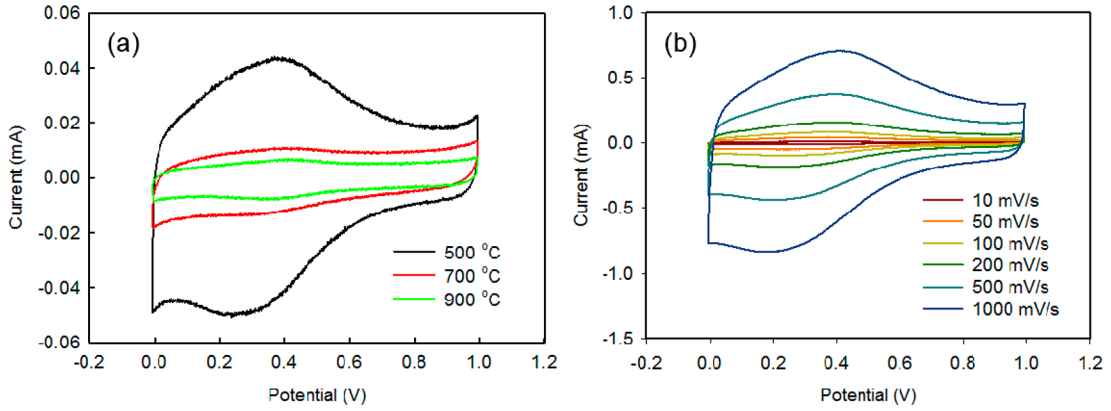

Figure 5. Cyclic voltammetry curves for the CNT ball-assembled electrodes. A 1 M H_2SO_4 solution was used as the electrolyte. A potential between 0 and 1 V was applied with a scan rate of (a) 50 mV/s and (b) various scan rates from 10 mV/s to 1 V/s.

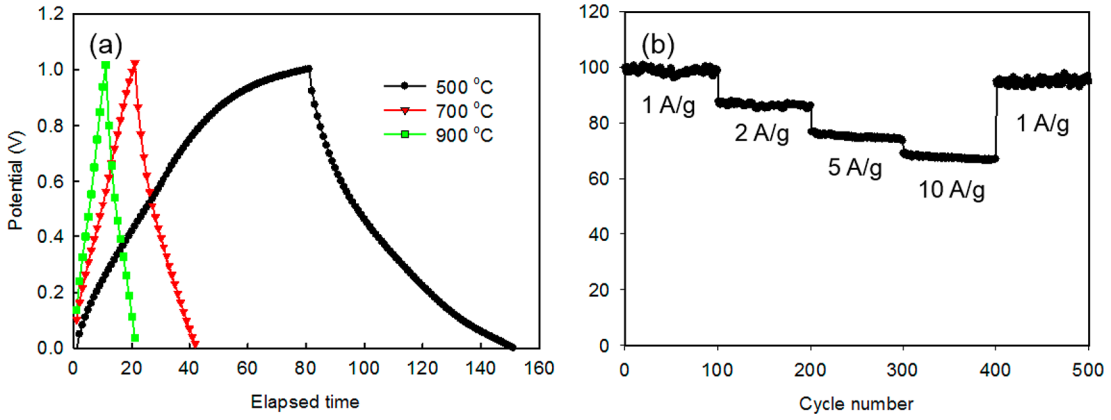

Figure 6. (a) Galvanostatic charge−discharge curves for the CNT ball-assembled electrode. The CNT balls were prepared at various temperatures. A 1 M H_2SO_4 solution was used as the electrolyte solution. A current density of 1 A/g was applied. (b) Capacitance retention of CNT ball electrodes at different current densities of from 1 A/g to 10 A/g.

dominant on the CNT balls, and the C−O groups decreased by half as the heat-treatment temperature increased to 900 °C. The quantity of −COO and C═O groups decreased by 5% and 18% at 900 °C, respectively. Desorption of the oxygenated groups from the CNTs at high temperatures has been previously reported.[34] In contrast to the BET result that revealed no effect on the macroscopic pore morphologies, the Raman result suggest that heat treatment leaves behind defects due to the desorption of oxygenated groups, and the process may also create additional defective bonds between CNTs.

The CNT balls were tested for their utility as electrodes in a supercapacitor electrode. The capacitive properties of the CNT balls prepared at various temperatures were characterized by standard cyclic voltammetry (CV) and galvanostatic charge−discharge techniques. Figure 5a shows the CV curves of CNT balls having one pair of redox peaks in addition to the electrochemical double-layer capacitive behavior. These peaks, which occurred within the range of 0.2−0.4 V, indicated the occurrence of a faradaic reaction of the oxygenated groups, that is, a reversible redox reaction of quinone to hydroquinone.[14,35] This feature is typically observed in CNTs having "oxygen-

dx.doi.org/10.1021/am404960r | ACS Appl. Mater. Interfaces 2014, 6, 706−711

containing" surface groups, and indicates the contribution of the pseudo-capacitive properties. Higher heat treatment temperatures resulted in a decrease in the area enclosed under the CV curve; the pseudo-capacitive peak almost disappeared for CNT balls treated at 900 °C; this result was consistent with the desorption of oxygenated groups during the high-temperature treatments, as indicated by the XPS results. Moreover, CV at various scan rates are shown in Figure 5b. The graphs reveal the redox peaks at the same potential by a faradaic reaction of oxygenated group, even at the scan rate of 1 V/s. This result reveals the stability of the oxygenated groups in the CNTs.

The galvanostatic charge−discharge curves are shown in Figure 6. The specific capacitance values of the CNT balls prepared at various temperatures were compared. The specific capacitance of the CNT balls was calculated from the discharge cycle of a typical voltage−time response curve using the equation

$$C = \frac{i\Delta t}{\Delta V m}$$

where C is the specific capacitance obtained from the discharge cycle under constant current charge/discharge measurements, i the constant current, Δt the discharge time, ΔV the potential range, and m the mass of the sample.[36] The calculated specific capacitance of the CNT balls prepared at 500 °C was 80 F/g. The specific capacitance was attributed to a lower pseudo-capacitance, as a result of desorption of the oxygenated groups at higher temperatures. Moreover, the capacitance retention was further evaluated for multiple steps at high charge/discharge current density (see Figure 6b). Each step comprised 100 charge/discharge cycles at different current rates from 1 A/g to 10 A/g. The capacitance of CNT balls remained at over 60% at a high current density of 10 A/g, and recovered to 95% of the initial capacitance when the current was reset to 1 A/g, suggesting excellent cycling performance and stability.

The CNT balls were tested as electrode materials in an effort to identify the influence of the spherical shape on the electrode performance properties. The capacitive properties of an electrode film composed of CNT ball assemblies and CNT films were compared. CNT ball electrodes were prepared by the evaporation of a CNT ball ethanol dispersion, whereas CNT films were obtained from CNTs dispersed in ethanol. The CNT films were made using the same CNT dispersion that was used for the CNT balls, and heat-treated at 500 °C. Figure 7 shows the specific capacitance values obtained at various current densities. At the low current density of 0.2 A/g, the specific capacitance values of the CNT balls and the CNT films were 81.6 and 58.6 F/g, respectively. The higher specific capacitance may have been attributed to a dense packing of CNTs in the CNT balls. A decrease in the capacitance with an increasing current density was observed for both electrodes. The presence of small pores, such as micropores and small mesopores, has been reported to have a detrimental effect on ion transport, thereby creating an electrical double layer on the pore surface. The specific capacitance obtained at 10 A/g was 48% of the value retained at a low current density (0.2 A/g) for the CNT balls and 43% for CNT films. The CNT ball electrodes showed a rate performance similar to that obtained from the CNT films. These results imply that the hierarchical porous structures of the CNT ball-assembled electrodes provided efficient mass transport of electrolyte ions during charging and discharging.

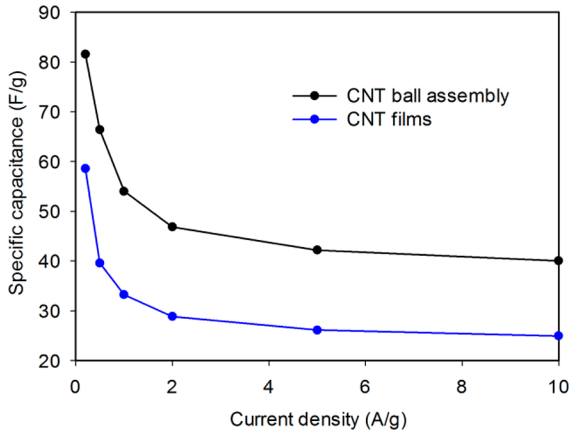

Figure 7. Specific capacitance of the CNT balls (black) and CNT films (blue) measured under different current densities between 0.2 A/g and 10 A/g.

CONCLUSION

Spherical carbon nanotube (CNT) assemblies, i.e., CNT balls, were fabricated by the evaporation of multiwalled carbon nanotube (CNT)-dispersed water/oil emulsion droplets. The emulsion-assisted assembly of CNTs induced compact packing of CNTs under capillary pressure during the evaporation of the droplets. CNT balls could then be redispersed in a solution to facilitate the preparation of a substrate coating. The coated film caused hierarchical pores among the CNTs and cavities among the CNT balls. Here, the size of the CNT balls could be controlled by varying the concentration of the CNT dispersion solution. Typically, the average size of the CNT balls obtained was in the range of 8−12 μm, and the BET surface area obtained for the CNT balls was 200 m^2/g. The effects of heat treatment on the pore structure and surface composition in the CNT balls were investigated. Heat treatment resulted in the removal of the covalently bound oxygenated groups from the CNTs, but heating did not affect the porosity of the CNT assemblies. The CNT ball assemblies were tested for their utility as a supercapacitor electrode. The pseudo-capacitance conveyed by the oxygenated groups yielded a specific capacitance of 80 F/g. The CNT ball electrodes showed a 40% higher specific capacitance and a slightly higher rate performance, compared to the CNT films. These results imply that the compact packing and hierarchical pore structure of the CNT balls may be a promising macrostructure for use in energy device applications. The emulsion-assisted methods described here may be extended to the fabrication of composite CNT balls from composite emulsion droplets to further enhance the capacitance.

ASSOCIATED CONTENT

Supporting Information

Morphologies and pore-size distribution of the CNT films. TGA curves for the CNT balls. This information is available free of charge via the Internet at http://pubs.acs.org.

AUTHOR INFORMATION

Corresponding Author

*E-mail: junhyuk@sogang.ac.kr.

Notes

The authors declare no competing financial interest.

■ ACKNOWLEDGMENTS

This work was supported by grants from the National Research Foundation of Korea (2013R1A1A2010973 and 2012M1A2A2671794). The Korea Basic Science Institute is also acknowledged for the SEM measurements.

■ REFERENCES

(1) Dubal, D. P.; Gund, G. S.; Lokhande, C. D.; Holze, R. *ACS Appl. Mater. Interfaces* **2013**, *5*, 2446−2454.
(2) Zhang, L.; Zhang, F.; Yang, X.; Leng, K.; Huang, Y.; Chen, Y. S. *Small* **2013**, *9*, 1342−1347.
(3) Frackowiak, E. *Phys. Chem. Chem. Phys.* **2007**, *9*, 1774−1785.
(4) Niu, Z. Q.; Zhou, W. Y.; Chen, J.; Feng, G. X.; Li, H.; Hu, Y. S.; Ma, W. J.; Dong, H. B.; Li, J. Z.; Xie, S. S. *Small* **2013**, *9*, 518−524.
(5) Bhaskar, A.; Deepa, M.; Rao, T. N. *ACS Appl. Mater. Interfaces* **2013**, *5*, 2555−2566.
(6) Frackowiak, E.; Gautier, S.; Gaucher, H.; Bonnamy, S.; Beguin, F. *Carbon* **1999**, *37*, 61−69.
(7) Gao, B.; Kleinhammes, A.; Tang, X. P.; Bower, C.; Fleming, L.; Wu, Y.; Zhou, O. *Chem. Phys. Lett.* **1999**, *307*, 153−157.
(8) Mink, J. E.; Hussain, M. M. *ACS Nano* **2013**, *7*, 6921−6927.
(9) Nutzenadel, C.; Zuttel, A.; Chartouni, D.; Schlapbach, L. *Electrochem. Solid State Lett.* **1999**, *2*, 30−32.
(10) Nardecchia, S.; Carriazo, D.; Ferrer, M. L.; Gutierrez, M. C.; del Monte, F. *Chem. Soc. Rev.* **2013**, *42*, 794−830.
(11) Baughman, R. H.; Zakhidov, A. A.; de Heer, W. A. *Science* **2002**, *297*, 787−792.
(12) Lee, S. W.; Yabuuchi, N.; Gallant, B. M.; Chen, S.; Kim, B. S.; Hammond, P. T.; Shao-Horn, Y. *Nat. Nanotechnol.* **2010**, *5*, 531−537.
(13) An, K. H.; Kim, W. S.; Park, Y. S.; Choi, Y. C.; Lee, S. M.; Chung, D. C.; Bae, D. J.; Lim, S. C.; Lee, Y. H. *Adv. Mater.* **2001**, *13*, 497−500.
(14) Frackowiak, E.; Metenier, K.; Bertagna, V.; Beguin, F. *Appl. Phys. Lett.* **2000**, *77*, 2421−2423.
(15) Du, X.; Wang, C. Y.; Chen, M. M.; Jiao, Y.; Wang, J. *J. Phys. Chem. C* **2009**, *113*, 2643−2646.
(16) Gamby, J.; Taberna, P. L.; Simon, P.; Fauvarque, J. F.; Chesneau, M. *J. Power Sources* **2001**, *101*, 109−116.
(17) Pandolfo, A. G.; Hollenkamp, A. F. *J. Power Sources* **2006**, *157*, 11−27.
(18) Ren, J.; Li, L.; Chen, C.; Chen, X.; Cai, Z.; Qiu, L.; Wang, Y.; Zhu, X.; Peng, H. *Adv. Mater.* **2013**, *25*, 1155−1159.
(19) Jin, Y.; Chen, H. Y.; Chen, M. H.; Liu, N.; Li, Q. W. *ACS Appl. Mater. Interfaces* **2013**, *5*, 3408−3416.
(20) Fan, X. M.; Yu, C.; Ling, Z.; Yang, J.; Qiu, J. S. *ACS Appl. Mater. Interfaces* **2013**, *5*, 2104−2110.
(21) Chen, T.; Qiu, L.; Yang, Z.; Cai, Z.; Ren, J.; Li, H.; Lin, H.; Sun, X.; Peng, H. *Angew. Chem., Int. Ed.* **2012**, *51*, 11977−11980.
(22) Cai, Z.; Li, L.; Ren, J.; Qiu, L.; Lin, H.; Peng, H. *J. Mater. Chem. A* **2013**, *1*, 258−261.
(23) Ericson, L. M.; Fan, H.; Peng, H. Q.; Davis, V. A.; Zhou, W.; Sulpizio, J.; Wang, Y. H.; Booker, R.; Vavro, J.; Guthy, C.; Parra-Vasquez, A. N. G.; Kim, M. J.; Ramesh, S.; Saini, R. K.; Kittrell, C.; Lavin, G.; Schmidt, H.; Adams, W. W.; Billups, W. E.; Pasquali, M.; Hwang, W. F.; Hauge, R. H.; Fischer, J. E.; Smalley, R. E. *Science* **2004**, *305*, 1447−1450.
(24) Vigolo, B.; Penicaud, A.; Coulon, C.; Sauder, C.; Pailler, R.; Journet, C.; Bernier, P.; Poulin, P. *Science* **2000**, *290*, 1331−1334.
(25) Bondavalli, P.; Delfaure, C.; Legagneux, P.; Pribat, D. *J. Electrochem. Soc.* **2013**, *160*, A601−A606.
(26) Futaba, D. N.; Hata, K.; Yamada, T.; Hiraoka, T.; Hayamizu, Y.; Kakudate, Y.; Tanaike, O.; Hatori, H.; Yumura, M.; Iijima, S. *Nat. Mater.* **2006**, *5*, 987−994.
(27) Chakrapani, N.; Wei, B. Q.; Carrillo, A.; Ajayan, P. M.; Kane, R. S. *Proc. Nat. Acad. Sci.* **2004**, *101*, 4009−4012.
(28) Moon, J. H.; Yi, G. R.; Yang, S. M.; Pine, D. J.; Bin Park, S. *Adv. Mater.* **2004**, *16*, 605.
(29) Everett, D. H.; Stone, F. S. (Colston Research Society). *The Structure and Properties of Porous Materials*; Butterworths: London, 1958; p xiv, 389 pp.
(30) Riggs, J. E.; Guo, Z. X.; Carroll, D. L.; Sun, Y. P. *J. Am. Chem. Soc.* **2000**, *122*, 5879−5880.
(31) Liu, L. Q.; Qin, Y. J.; Guo, Z. X.; Zhu, D. B. *Carbon* **2003**, *41*, 331−335.
(32) Li, M.; Boggs, M.; Beebe, T. P.; Huang, C. P. *Carbon* **2008**, *46*, 466−475.
(33) Wang, H.; Zhou, A.; Peng, F.; Yu, H.; Yang, J. *J. Colloid. Interface Sci.* **2007**, *316*, 277−283.
(34) Kundu, S.; Wang, Y. M.; Xia, W.; Muhler, M. *J. Phys. Chem. C* **2008**, *112*, 16869−16878.
(35) Kim, I. H.; Kim, J. H.; Kim, K. B. *Electrochem. Solid State Lett.* **2005**, *8*, A369−A372.
(36) Pang, S. C.; Anderson, M. A.; Chapman, T. W. *J. Electrochem. Soc.* **2000**, *147*, 444−450.